Bioactive Materials 15 (2022) 29–43

Contents lists available at ScienceDirect

Bioactive Materials

journal homepage: www.keaipublishing.com/en/journals/bioactive-materials

Injectable cartilage matrix hydrogel loaded with cartilage endplate stem cells engineered to release exosomes for non-invasive treatment of intervertebral disc degeneration

Liwen Luo [a,b,1], Junfeng Gong [a,1], Zhouguang Wang [c,d,*,1], Yao Liu [e,1], Jiaming Cao [f], Jinghao Qin [a], Rui Zuo [a], Hongyu Zhang [g], Shuai Wang [h], Ping Zhao [i], Di Yang [b], Mengjie Zhang [j,k], Yanqiu Wang [a], Junfeng Zhang [l], Yue Zhou [a], Changqing Li [a,**], Bing Ni [j,k,***], Zhiqiang Tian [b,i,****], MingHan Liu [a,*****]

[a] Department of Orthopaedics, Xinqiao Hospital, Army Medical University (Third Military Medical University), Chongqing, China
[b] Institute of Immunology, PLA, Army Medical University (Third Military Medical University), Chongqing, China
[c] Molecular Pharmacology Research Center, School of Pharmaceutical Science, Wenzhou Medical University, Wenzhou, 325000, Zhejiang, China
[d] Department of Orthopaedics, The Second Affiliated Hospital and Yuying Children's Hospital of Wenzhou Medical University, Wenzhou, 325000, Zhejiang, China
[e] Department of Pharmacy, Daping Hospital, Army Medical University (Third Military Medical University), Chongqing, China
[f] Institute of Geophysics and Geomatics, China University of Geosciences, Wuhan, China
[g] Department of Emergency, Second Affiliated Hospital of Chongqing Medical University, Chongqing, China
[h] Institute of Pathology and Southwest Cancer Center, Southwest Hospital, Army Medical University (Third Military Medical University), Chongqing, China
[i] State Key Laboratory of Silkworm Genome Biology, Biological Science Research Center, Southwest University, Chongqing, China
[j] Department of Pathophysiology, College of High Altitude Military Medicine, Army Medical University, Chongqing, China
[k] Key Laboratory of Extreme Environmental Medicine, Ministry of Education of China, Army Medical University (Third Military Medical University), Chongqing, China
[l] Institute of Hepatopancreatobiliary Surgery, Chongqing General Hospital, University of Chinese Academy of Sciences, Chongqing, China

ARTICLE INFO

Keywords:
Intervertebral disc degeneration
Engineered exosomes
Hydrogels
Extracellular matrix of costal cartilage
Sphingosine kinase 2

ABSTRACT

Low back pain, mainly caused by intervertebral disc degeneration (IVDD), is a common health problem; however, current surgical treatments are less than satisfactory. Thus, it is essential to develop novel non-invasive surgical methods for IVDD treatment. Here, we describe a therapeutic strategy to inhibit IVDD by injecting hydrogels modified with the extracellular matrix of costal cartilage (ECM-Gels) that are loaded with cartilage endplate stem cells (CESCs). After loaded with CESCs overexpressing Sphk2 (Lenti-Sphk2-CESCs) and injected near the cartilage endplate (CEP) of rats in vivo, ECM-Gels produced Sphk2-engineered exosomes (Lenti-Sphk2-Exos). These exosomes penetrated the annulus fibrosus (AF) and transported Sphk2 into the nucleus pulposus cells (NPCs). Sphk2 activated the phosphatidylinositol 3-kinase (PI3K)/p-AKT pathway as well as the intracellular autophagy of NPCs, ultimately ameliorating IVDD. This study provides a novel and efficient non-invasive combinational strategy for IVDD treatment using injectable ECM-Gels loaded with CESCs that express Sphk2 with sustained release of functional exosomes.

Peer review under responsibility of KeAi Communications Co., Ltd.

* Corresponding authors. Molecular Pharmacology Research Center, School of Pharmaceutical Science, Wenzhou Medical University, Wenzhou, 325000, Zhejiang, China.
** Corresponding author. Department of Orthopaedics, Xinqiao Hospital, Army Medical University, Chongqing, China.
*** Corresponding author. , Department of Pathophysiology, College of High Altitude Military Medicine, & Key Laboratory of Extreme Environmental Medicine, Ministry of Education of China, Army Military Medical University, Chongqing, 400038, China.
**** Corresponding author. Institute of Immunology, Army Medical University, Chongqing, 400038, China.
***** Corresponding author. Department of Orthopaedics, Xinqiao Hospital, Army Medical University, Chongqing, China.
E-mail addresses: wzhouguang@gmail.com (Z. Wang), changqli@163.com (C. Li), nibing@tmmu.edu.cn (B. Ni), tzhiq009@163.com (Z. Tian), liuminghan2008@hotmail.com (M. Liu).
[1] Authors contribute equally.

https://doi.org/10.1016/j.bioactmat.2021.12.007
Received 10 June 2021; Received in revised form 21 November 2021; Accepted 13 December 2021
Available online 21 December 2021

1. Introduction

More than 80% of the world's population currently suffers from lower back pain, mainly caused by intervertebral disc degeneration (IVDD) [1,2]. Surgery is the most extensive and effective for the treatment of IVDD. Invasive surgical treatment brings great pain and burdens to the patients; moreover, it greatly increases the societal medical expenses; therefore, non-invasive treatment for disc degeneration is urgently needed [3]. Exosome-based drug delivery and targeting are promising medical strategies for the treatment and prevention of a variety of diseases [4,5], moreover, injectable hydrogel materials binding to exosomes have been previously used as non-surgical treatments for cartilage regeneration [6]. Engineering exosomes loaded with miRNAs or synthesized proteins can enhance the therapeutic effect *in vitro* [7]. Exosomes from the stem cells of patients can treat IVDD via autologous reinfusion, which reduces the chance of immune rejection. Furthermore, lentivirus-engineered cells are an effective high-throughput protein drug production device [8]. Thus, we propose that an injectable hydrogel combined with lentivirus-engineered cartilage endplate stem cells (CESCs) may not only be a potential non-surgical treatment, but may also increase the long-term therapeutic effect of IVDD through the continuous and stable production of engineered exosomes.

Nanomaterial exosomes are extracellular vesicle structures between 30 and 150 nm in diameter that are released from the fusion of cavity vesicles with the plasma membrane [9]. Exosomes already play an important role in attenuating kidney and heart ischemia-reperfusion injury [10–12], accelerating the repair of damaged liver cells [13], and inhibiting the progression of both neurodegenerative diseases and IVDD [14]. The main mechanism by which exosomes participate in intercellular communication and damaged tissue repair is via the transportation of functional components, such as proteins and small RNAs [15–17]. Engineered exosomes loaded with small RNAs, proteins, or compounds can more effectively inhibit tumor progression and improve inflammation and regeneration [18,19]. Currently, there are no studies on engineered exosomes derived from lentivirus-engineered cells for IVDD treatment. Therefore, we propose a new direction for IVDD treatment that includes constructing lentivirus engineered CESCs to facilitate the generation of engineered exosomes; this may be a very promising and effective treatment for IVDD.

In the clinical application of exosomes, the current major challenges are retaining and stabilizing them in vivo. Hydrogel-coated exosomes can delay the degradation of exosomes in vivo, [20] however, exosomes cannot be produced sustainably and steadily over a long time. Two-dimensional (2D) plastic tissue culture dishes limit the surface area for cell growth as well as cell–cell and cell–extracellular matrix interactions as they do not represent the body's environment. However, hydrogels can be used for three-dimensional (3-D) cultures of mesenchymal stem cells (MSCs), thus generating exosomes. This largely represents the in vivo conditions and the MSC are induced to produce more exosomes by promoting intercellular interactions [21]. Temperature controlled rat tail collagen hydrogels (Gels) can form the gel quickly at 37 °C, thus preventing cell flow and providing a skeleton structure needed for cell growth [22]. The extracellular matrix of rat costal cartilage (ECM-Gels) possess various factors, such as growth factors and chemokines [23], that are needed to support the growth, differentiation, and migration of CESCs that are present in the cartilage endplate (CEP) located on both the upper and lower sides of the intervertebral disc (IVD). Currently, the role of injectable hydrogels modified by costal cartilage extracellular matrix (ECM-Gels) has not been studied in regulating cell growth. IVD has been identified as an immune privilege organ. Annulus fibrosus (AF) and CEP construct the blood-nucleus pulposus (NP) barrier to isolate the NP from the host immune system [24,25]. Therefore, it is urgent to find a way to delay IVDD without destroying the AF. CESCs in CEP have the capability of releasing exosomes in situ [26]. Constructing ECM-Gels loaded with engineered CESCs near the CEP may provide a solution for the continuous release of engineered exosomes without destroying the normal structure of the AF, therefore facilitating and continuously enhancing the treatment of IVDD as well as accelerating the repair of degenerated IVD.

Sphingosine kinase 2 (Sphk2) activates sphingosine to form sphingosine-1-phosphate (S1P) and regulates many biological functions, such as cell survival, migration, and invasion, as well as angiogenesis, differentiation, and the immune cell response via the p-ERK1/2, p-AKT, and autophagy signaling pathways [27–29]. In neuronal ischemia-reperfusion injury, Sphk2 significantly inhibited neuronal damage by activating autophagy [29,30]. Moreover, exosomes can transport Sphk2 to repair damaged liver cells [8]. We confirmed that Sphk2 was an inhibitor of IVDD, and presented a novel therapeutic direction for IVDD treatment in which CESCs overexpressing Sphk2 are encapsulated in an ECM-Gels. This study provides the possibility for the clinical application of engineered Lenti-Sphk2-Exos to transport Sphk2, activating NPC autophagy and treating IVDD.

2. Materials and methods

2.1. Reagents and antibodies

The Sphk2 inhibitor (ABC294640, cat. no. S7174) and 3-methyladenine (3-MA, cat. no. S2767) were obtained from Selleck (Shanghai, China). An AKT inhibitor (LY294002, cat. no. S1737) was obtained from Beyotime (Shanghai, China). Antibodies against GAPDH, IL-6, IL-1, MMP1, p21, p16, Beclin-1, p-AKT, Sphk2, TSG101, HSP70, and Alix were purchased from Proteintech (Wuhan, China). Antibodies against AKT, JNK/p-JNK, and NFκB/p-NFκB were obtained from Abcam (Cambridge, MA, USA). Antibodies against LC3A/B were purchased from KleanAB (Shanghai, China). Antibodies against LC3B (cat. no. bs-4843R) were purchased from Bioss (Beijing, China). Collagenase II (cat. no. A004202) was purchased from Sangon Biotech (Shanghai, China). *Tert*-butyl hydroperoxide (TBHP, cat. no. 458139),PKH26(cat. no. MINI26), and PKH67(cat. no. PKH67GL) were obtained from Sigma (St. Louis, MO, USA). 1,1′-Dioctadecyl-3,3,3′,3′-tetramethylindotricarbocyanine iodide (DIR) was obtained from Invitrogen (Carlsbad, CA, USA). MSC osteogenic differentiation medium (cat. no. MUBMX-90021), chondrogenic differentiation medium (cat. no. MUCMX-9004), and adipogenic differentiation medium (cat. no. MUBMX-90031) were provided by Cyagen (Guangzhou, China).

2.2. Patient's tissue, rat intervertebral disc degeneration model and reagent treatment

All human intervertebral disc tissues (20 patients) were collected from patients undergoing elective intervertebral removal surgery. The work was given official approval by the Ethics Committee of the Xinqiao Hospital of Army Medical University (AF/SC-08/1.0). Written informed consent was obtained from patients or their relatives prior to tissue collection. Male rats were provided by the Animal Experimental Center of the Army Medical University (ChongQing, China). Five young male rats (aged three-four weeks) were used to isolate CESCs and NPCs. IVDD was established in rats according to previously described methods [31]. Six adult male rats were divided into two groups to verify that CESC-exosomes could penetrate the AF of the IVD and enter the NPCs. Three rats in the control group were injected with unlabeled exosomes, and three rats in the test group were injected with DIR-labeled exosomes. A total of 12 male rats (two-three weeks old) were divided into three groups: control, CESCs + Gels, and CESCs + ECM-Gels groups to verify that ECM-Gels were more beneficial for cell growth. Forty eight rats (two-three weeks old) were divided into four groups: control, puncture, puncture + CESCs + ECM-Gels, and puncture + Lenti-Sphk2-CESCs + ECM-Gels groups. Another 12 adult male rats (12 weeks old) were divided into three groups: control, puncture, and puncture + exosome groups. Another 20 adult male rats (12 weeks old) were used for the rat IVDD model, which were divided into five groups:

control, puncture, puncture + Lenti-Sphk2-exosome group, puncture + Lenti-Sphk2-exosome + 3-MA, and puncture + Lenti-Sphk2-exosome + AKT inhibitor (LY294002) groups. After anesthetization with 5% chloral hydrate, the entire AF layer in the caudal discs (C5/6, C6/7, and C7/8) were randomly transversely punctured with a 21G skin puncture needle for 30 s. After suturing the wound, a 31G microsyringe was used to treat the intervertebral disc with 10 μL Lenti-Sphk2-exosomes (40 μg), and either 10 μL 3-MA (20 μmol/ml) or 10 μL LY294002 (20 μmol) on the opposite side of the puncture site according to the above groups. The specific method was to inject Lenti-Sphk2-exosomes into the corresponding sites, followed by injecting the inhibitor 3-MA or LY294002 5–10 min later. Six weeks after surgery in the IVDD rats the discs were harvested. Animal use and experimental procedures met the requirements of the Guidelines for the Care and Use of Laboratory Animals of the National Institutes of Health and was given official approval by Animal Ethics Committee Army Medical University (no,SYXK(yu) 2017–0002).

2.3. Cartilage endplate stem cell and nucleus pulposus cell isolation and characterization

Five young rats (2–4 weeks) were anesthetized with 5% chloral hydrate and sacrificed. Six to eight segments of caudal vertebrae NP tissues were obtained from the caudal root with a surgical tip blade. After the surrounding soft tissues were removed, the AF and medullary cavity on both sides of the CEP were excised as much as possible to obtain CEP. The NP and CEP tissues were cut into 1 mm^3 pieces and placed in different centrifuge tubes. A total of 6 mL of 0.2% collagenase II was added, and the tubes were gently shaken at 37 °C for 1–2 h. After the tissues were digested into fine particles, they were filtered through a 70 μm filter. Then, the NP tissues and CEP tissues were inoculated into a medium dish (diameter 10 cm) and cultured in 6 mL DMEM/F12 complete medium (SH30023.01, HyClone) containing 20% fetal bovine serum (FBS, A6903FBS-500, Invitrogen) at 5% CO2 and 37 °C. 5 mL DMEM/F12 containing 20% serum was added to two medium dishes on the second and third days. The cells were digested and collected with 0.25% trypsin-EDTA when they reached 80–90% confluence. The cells were harvested, and subsequent generations were used in our experiments.

2.4. Osteogenic, adipogenic, and chondrogenic differentiation

CESCs were cultured in 6-well plates for osteogenic differentiation. The osteogenic differentiation medium (MUBMX-90021, Cyagen Biosciences, Guangzhou, China) was changed every 3 days for 2–3 weeks. The cells were washed twice with phosphate buffered saline (PBS), then fixed with 2 mL of 4% neutral formaldehyde solution for 20 min at room temperature, and then stained with 1% Alizarin Red S solution for 30 min. Osteogenesis was evaluated under a microscope (Olympus, Japan). CESCs were cultured in 6-well plates for adipogenic differentiation. The adipogenic differentiation medium was replaced every 3 days, and the cells were then cultured with medium B (MUBMX-90031, Cyagen) for 1 d. This cycle was repeated for a total of 3 weeks. The cells were washed twice with PBS, fixed with 2 mL of 4% neutral formaldehyde solution for 20 min, and stained with Oil Red O working solution for 30 min. Adipogenesis was then evaluated under a microscope. For chondrogenic differentiation, 3–4 1×10^5 CESCs were centrifuged at 250 × *g* for 5 min and incubated with chondrogenic differentiation medium (MUCMX-9004, Cyagen) in a centrifuge tube at 37 °C in 5% CO2 for 48 h. When the cells were gathered, the bottom was flicked to detach the cartilage ball from the bottom of the tube, then the cells were cultured in chondrogenic differentiation medium for 21 days. To estimate chondrogenesis, the chondrified micromass was fixed with 4% formaldehyde, embedded in paraffin, sliced at a thickness of 4 μm, and then stained with Alcian Blue for observation under a microscope.

2.5. Preparation of hydrogels modified with costal cartilage extracellular matrix

The rats were anesthetized with 5% chloral hydrate (2 mL) and killed by breaking their necks. The tail skin was cut open, and the tail tendon was removed and cleaned with saline. The tail tendon was cut into pieces and placed in 150 mL of 0.5% acetic acid. The tendon was then shaken and dissolved for 48 h at 4 °C. It was then centrifuged at 12,000 rpm and the supernatant was added to a 10% NaCl solution to precipitate the collagen. An appropriate volume of HCL (0.2 mM) was added to dissolve the supernatant, and the supernatant was stored at 4 °C for later use.

The costal cartilage of the rats (aged 2–3 weeks) was removed, cut into pieces and then grinded with a tissue grinder (70 Hz, 2 min, 3 times) (JXFSTPRP-CL, Shanghai Jing Xin, Shanghai, China). Tissue homogenate was obtained, and 4 mL of medium was added for dilution. Then the filtrate was collected through a 0.22-μm filter to obtain the chondrocyte extracellular matrix. 50 μL of cartilage extracellular matrix was added to 700 μL of hydrogel, and 250 μL of 1×10^5 CESCs were added. After mixing, the gel was formed over 5–10 min at 37 °C. This constructed the hydrogel loaded with CESCs that were modified by the cartilage extracellular matrix.

2.6. Exosome isolation and characterization

CESCs were harvested and cultured in T75 flasks containing 10% FBS. After the cells reached 60–70% confluence, they were further cultured for another 48–72 h in serum-free DMEM/F12 medium (SH30023.01, HyClone). Then the culture medium supernatant was collected. Exosomes were extracted by ultracentrifugation, as previously described [32,33]. The centrifugation steps were as follows: 300 × *g* for 10 min to remove live cells, then 2000×*g* for 10 min to remove dead cells, followed by 10,000 × *g* for 30 min to remove cell debris, and finally 100,000 × *g* for 70 min. The supernatant was then discarded to obtain exosome pellets. Exosomes were washed with PBS, filtered through a 0.22-μm filter, and centrifuged at 100000 × *g* for another 70 min. After further dilution with 200 μL of sterile PBS, 5 μL of PKH26, PKH67, or DIR was added to 500 μL of the diluent to form the reaction liquid; then 100 μL of exosomes was added to the reaction liquid. After 10 min, 5% bovine serum albumin (BSA) was added to stop the reaction, and exosomes labeled with different membrane dyes were obtained. The size and concentration of exosomes were measured by nanoparticle tracking analysis (NTA, Wayen Biotechnologies, Shanghai). The morphology of exosomes was examined by electron microscopy, and the purity and characteristics were analyzed via Western blot (WB) analysis based on the expression of exosome markers (TSG101, HSP70, and Alix).

2.7. Transmission electron microscopy

The cells were digested and isolated using trypsin and immobilized with 2% glutaraldehyde at 4 °C for 2 days. The samples were treated with 1% osmium for 30 min. Ultrathin sections were prepared by gradient dehydration in 50–100% ethanol and incubated in a mixed solution of 100% acetone/Epon 812 (Shell Chemical Co., Houston, TX, USA). Then, the ultrathin sections were dyed with 5% uranyl acetate for 30–60 min and washed 3 times with double-distilled water. The ultrathin sections were then dyed with lead citrate for 10 min, and washed a further 3 times with double-distilled water. Then the samples were observed by transmission electron microscopy (TEM).

2.8. Real-time quantitative reverse transcriptase polymerase chain reaction

Total RNA was extracted from cells using the TRIzol method according to a previously described experimental procedure [34]. The PrimeScript RT reagent kit (Takara, Japan) and SYBR Premix Ex TaqTM

(Takara, Japan) were used for the reverse transcription of complementary DNA and quantitative amplification as previously described [35]. The rat and human primers used for real-time quantitative polymerase chain reaction (RT-qPCR) were synthesized and provided by Thermo Fisher Scientific. The 2-ΔΔCt method was used to analyze target gene expression levels and compare differences.

2.9. Western blotting

Cells were collected and lysed in RIPA buffer containing a cocktail of the protease inhibitor PMSF alongside other phosphatase inhibitors (Beyotime, Shanghai, China) to extract total proteins. Nuclear and cytoplasmic proteins were isolated using a nuclear and cytoplasmic extraction kit (Beyotime). Protein concentration was determined, and a 4 × SDS-PAGE loading buffer was added to the samples. Electrophoresis

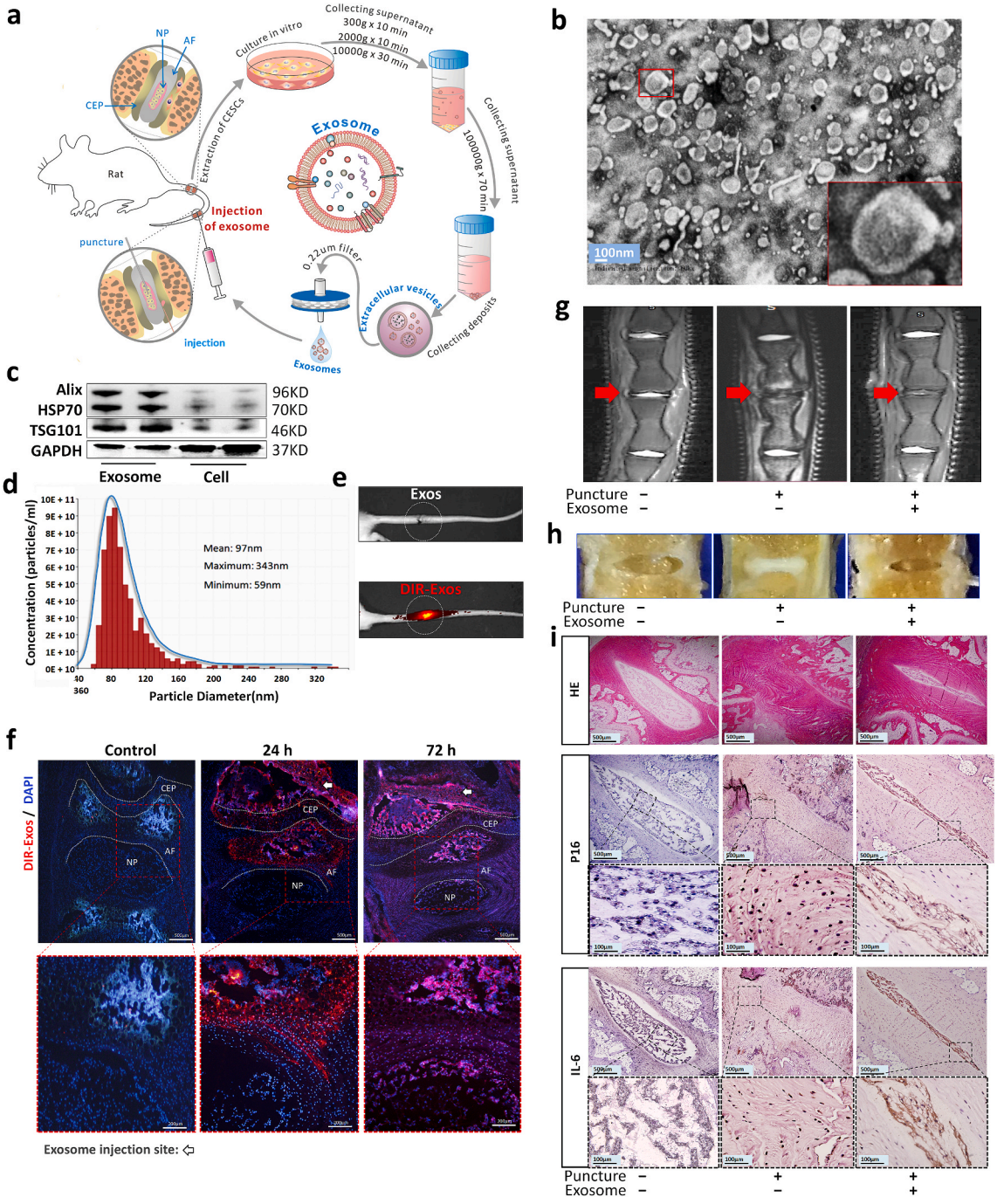

Fig. 1. Cartilage endplate stem cell-exosomes can cross the annulus fibrosus to alleviate disc degeneration
a) Flowchart of exosome extraction and treatment of intervertebral disc degeneration (IVDD). b-d) Transition electron microscopy images, western blotting analysis, and nanotracking analyses were used to identify exosomes. e) In vivo imaging of rat intervertebral discs and the vertebral segments treated with unlabeled exosomes (Exos, 10 μg) or DIR-labeled exosomes (DIR-Exos, 10 μg). f) Fluorescence microscope observation of the above-mentioned intervertebral disc tissue sections at 24 or 72 h. g) The representative magnetic resonance images of rat intervertebral discs treated by NC, puncture, and puncture + cartilage endplate stem cell-Exos. h) The morphology of intervertebral disc tissue at 6 weeks after being treated as above. i) The representative images of hematoxylin and eosin and immunohistochemistry stainings of P16 and IL-6 in the rat disc samples after being treated as above.

was performed at 150 V with 4–20% gradient gels. Semidry transfer electrophoresis was performed for 7 min at 25 V. After the membrane was sealed, the antibodies were diluted according to the manufacturer's instructions and added to the membrane. They were then incubated at 4 °C overnight with oscillation. The membrane was washed, and then diluted secondary antibodies were added and incubated for 1.5 h. The enhanced chemiluminescence working solution (Millipore, MO, USA) was prepared by mixing solutions A and B at a ratio of 1:1. The working solution was placed on a film surface; then the film was placed in an imaging system (Bio-Rad, USA) and pictures were taken.

2.10. Immunohistochemical staining

The IVD and CEPs of clinical patient samples were isolated, fixed with 4% paraformaldehyde, decalcified, and sectioned in paraffin. The samples were baked, dewaxed, hydrated, and then sealed at room temperature for 30 min with 10% H_2O_2, after which the samples were rinsed again with PBS. After antigen repair, normal goat serum block solution was added the samples were incubated at room temperature for 10 min. A total of 50 μL of diluted primary antibody (Sphk2, 1:200; P16, 1:200) was added and incubated overnight at 4 °C. The samples were washed with PBS three times, and the biotinylated secondary antibody was added and incubated for a further 10 min at 37 °C. The samples were then rinsed another three times with PBS, and reagent D was added reacted with the samples at room temperature for 10 min. DAB reagent was then used to stain the sections for microscopy analysis; then, the sections were dehydrated and underwent transparence treatment before being sealed, observed, and then photographed under a microscope (Olympus, Japan).

2.11. Immunofluorescence staining

Cells in culture dishes or hydrated tissue sections were then obtained. The samples were washed with PBS three times, incubated in 10% hydrogen peroxide/formaldehyde solution for 30 min at room temperature, permeabilized in 0.2% Triton for 5 min, sealed with 5% BSA for 30 min, and then incubated overnight at 4 °C with 50 μL of diluted primary antibody. The specimens were then washed with PBS three times again and incubated with fluorescently labeled secondary antibody (1:300 dilution) at 37 °C for 60 min. Nuclei were stained for 3–5 min with 0.2 g/mL DAPI (Beyotime, Nantong, China). Images were captured using a fluorescence microscope (Olympus, Japan) and laser confocal microscope (Lexia, Japan).

2.12. Correlation analysis of Pfirrmann grading and Sphk2 expression

According to the T2-weighted images, the degree of IVDD was graded using the modified Pfirrmann grading method. The correlation between mRNA and protein of Sphk2 expression in the corresponding CEP and NP was then analyzed.

2.13. Lentiviral transfection

Sphk2 was overexpressed and knocked down via lentiviruses produced by GenePharma (Shanghai, China). Lenti-*Sphk2* or Lenti-sh*Sphk2* were used to transfect NPCs or CESCs that had reached 30% confluence after 12 h of culture. After culturing with 10 μg/mL puromycin for 7 days, WB and RT-qPCR were used to determine the transfection efficiency and protein expression levels. CESCs transfected with Lenti-*Sphk2* or Lenti-*shSphk2* could produce Lenti-*Sphk2* engineered exosomes (Lenti-Sphk2-Exos) or Lenti-shSphk2 engineered exosomes (Lenti-shSphk2-Exos).

2.14. Senescence-associated β-galactosidase staining

A Senescence-associated β-galactosidase (SA-β-gal) staining kit (Beyotime, Shanghai, China) was used to detect senescence. The level of SA-gal activity was indicated by a blue stain, which becomes darker as the cells age.

2.15. Flow cytometry to detect apoptosis and identify cartilage endplate stem cells

CESCs were digested and collected using 0.25% trypsin-EDTA. The cells were washed with 1 × PBS 3 times and centrifuged at 300 × *g* for 5 min to remove the remaining trypsin, then 5 μL of antibody was added to each sample. To identify CESCs, antibodies against CD29 (102,201, Biolegend, San Diego, CA, USA), CD90 (202,503, BioLegend), and CD45 (103,107, Biolegend) were used. After the cells were incubated at room temperature for 30 min, they were washed with PBS and the percentage of CESCs was detected and analyzed by flow cytometry (BD FACSCalibur, USA).

2.16. Hematoxylin-eosin staining

Paraffin-embedded tissue sections were dewaxed, hydrated, and stained with hematoxylin solution for 3–5 min. After the sections were washed with PBS, 1% HCL was used to differentiate the tissue sections. Eosin solution was then added, and the cells were incubated for 1 min. Then the sections were dehydrated, cleared, sealed, and observed and photographed under a microscope (Olympus, Japan).

2.17. Magnetic resonance imaging

Six weeks after the operation, a 7.0 T animal magnet (Bruker Pharmascan, Germany) was used to detect the signal and structural changes in the disc based on the sagittal T2-weighted images. The parameters of the T2-weighted sections were set as previously described [36]. The magnetic resonance imaging (MRI) images of patients were evaluated in a blinded manner according to IVDD-modified Pfirrmann MRI grades [37].

2.18. Statistical analysis

All data are presented as the mean ± standard deviation (S.D) of at least three independent experiments. One-way analysis of variance (ANOVA) followed by Tukey's test was used for comparisons between the two groups. Results were analyzed and compared using GraphPad Prism 7.0 (GraphPad Software Inc., CA, USA). Statistical significance was set at $p < .05$.

3. Results and discussion

3.1. Cartilage endplate stem cell-derived exosomes penetrate the annulus fibrosus to alleviate intervertebral disc degeneration

A flow chart of exosomes used for treating IVDD is shown in Fig. 1a. The CEP is located on both sides of the IVD and plays an important role in maintaining the structural integrity of the IVD as well as repairing degeneration. We extracted CESCs from 2- to 3-week-old rats and identified the CESCs by using osteogenic, chondrogenic, and adipogenic differentiation and flow cytometry (Supplementary Figs. 1a–b). The cells from the CEP had distinct stem cell properties [38], high expression of CD29 and CD90, and low expression of CD45. The CESC-Exos were extracted, and the morphology, size, and concentration of these exosomes were examined by TEM, WB, and NTA analysis (Fig. 1b–d). To verify that exosomes can enter NPCs, we injected unlabeled or DIR-labeled exosomes (DIR-Exos) between the CEP and IVD. After 6 h, the rat tail was imaged, and exosomes were found within the IVD (Fig. 1e). Moreover, fluorescence imaging of frozen sections at 24, and 72 h revealed that DIR-labeled exosomes could gradually migrate into the NPCs from the injection site between the CEP and AF (Fig. 1f). In

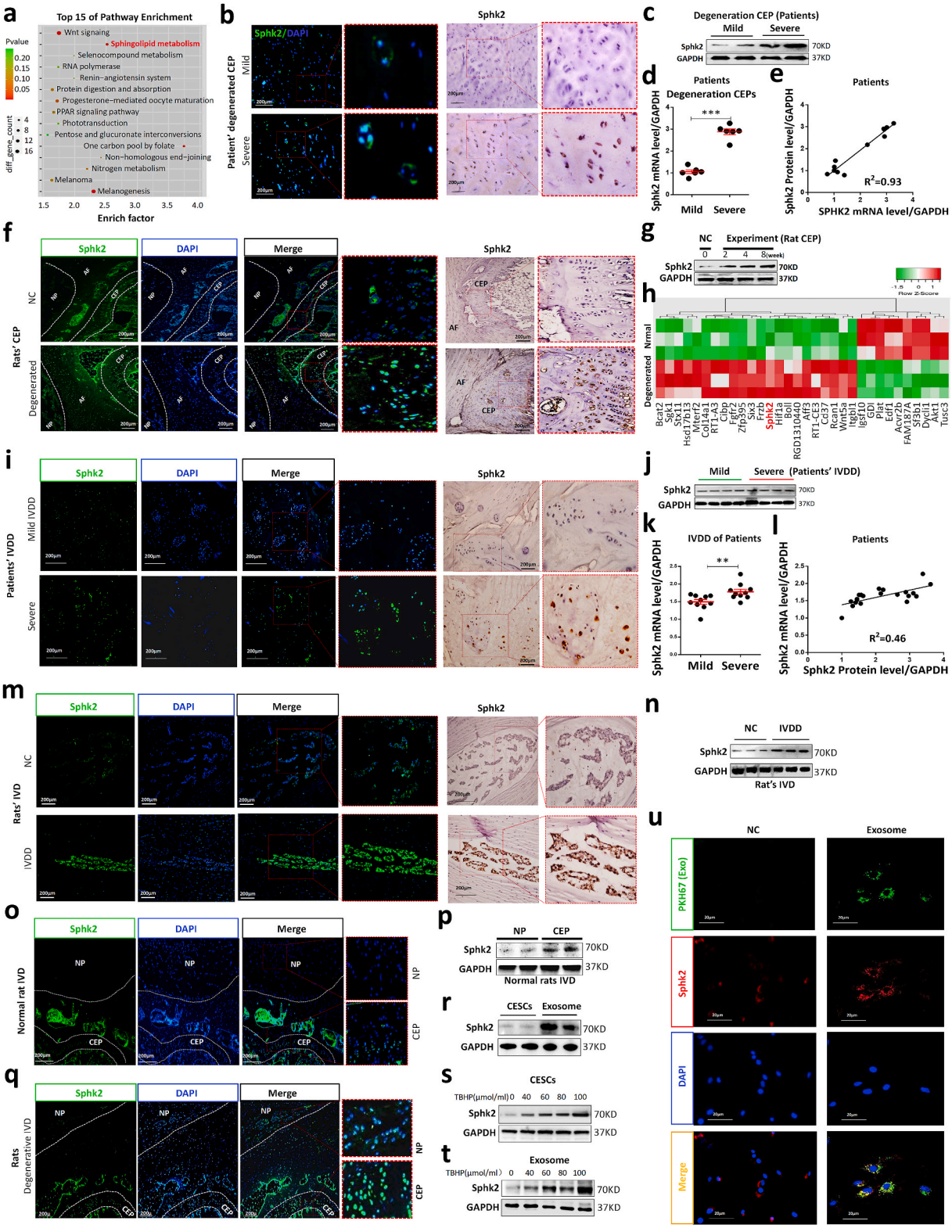

(caption on next page)

Fig. 2. Expression of Sphk2 in degenerated cartilage endplate is higher than that of the nucleus pulposus and Sphk2 can be transported into nucleus pulposus cells via exosomes secreted by cartilage endplate stem cells
a) The Kyoto encyclopedia of genes and genomes enrichment analysis of differences in genes between patients with normal and degenerate cartilage endplates (CEPs) (GSE153761, https://www.ncbi.nlm.nih.gov/). b-c) The representative immunofluorescence and immunohistochemical staining of Sphk2 and western blotting analysis of Sphk2 in patients with mild and severe degenerated CEP tissues. d) The mRNA levels of Sphk2 in the CEP specimens of patients. e) Correlation analysis of protein levels and mRNA levels of Sphk2 in the CEP specimens of patients. f) The representative immunofluorescence and immunohistochemical staining of Sphk2 in rat CEP specimens. g) The western blotting analysis of Sphk2 in normal and degenerated CEP rat specimens at 2, 4, and 6 weeks after the acupuncture disc experiment. h) Heat map analysis evaluates the differential expression of Sphk2 in normal or degenerated rat intervertebral discs (GSE126883, https://www.ncbi.nlm.nih.gov/). i-j) Representative immunofluorescence staining, immunohistochemical staining, and Western blot analysis detects Sphk2 and degenerated clinical IVD specimens. k) mRNA level of *Sphk2* in degenerated clinical IVD specimens. l) Correlation analysis of protein and mRNA levels of Sphk2 in clinical NP specimens based on modified Pffirrmann classification. m-n) Immunofluorescence staining, immunohistochemical staining and Western blot analysis of Sphk2 in both normal and degenerated IVD tissues of rats. o-p) Expression of Sphk2 in both the normal NP and CEP of rats was analyzed by immunofluorescence staining and Western blot analysis. q) Expression of Sphk2 in rat degenerative NP and CEP was analyzed by immunofluorescence staining. r) Representative western blots of Sphk2 in cartilage endplate stem cells (CESCs) and exosomes. s) Western bloting assay of Sphk2 in the CESCs treated with different concentrations of TBHP (0, 40, 60, 80, and 100 μmoL/ml) for 72 h. t) Sphk2 expression in exosomes derived from CESCs treated with different concentrations of TBHP (0, 40, 60, 80, and 100 μmoL/ml) for 72 h. u) Double immunofluorescence of Sphk2 (red) and exosomes (green) in NP cells. NC: Normal Control. ns: $p > .05$; *$p < .05$; **$p < .01$; ***$p < .001$.

other words, at 24 h, exosomes were mainly gathered near the AF, but at 72 h, some exosomes had entered NPCs. The rats were divided into three groups: the NC, puncture, and puncture + exosome groups; these were used to confirm the efficacy of CESC-Exos for IVDD. Moreover, MRI results suggested that puncture exacerbated the degeneration of IVDs, and that exosomes alleviated disc degeneration (Fig. 1g). The general morphology of the rat vertebrae was observed at 6 weeks. I**nterverte-bral d** isc degeneration was observed in longitudinal sections, and the severity of disc degeneration was similar to that observed using MRI (Fig. 1h). HE and immunohistochemistry stains of P16 and IL-6 also showed that CESC-Exos inhibited puncture-induced IVDD (Fig. 1i).

3.2. Exosomes secreted by cartilage endplate stem cells can transport Sphk2 into nucleus pulposus cells

The gene chip results were analyzed (**GSE153761**, https://www.ncbi.nlm.nih.gov/) to determine the metabolic differences between normal and degenerated CEP. Kyoto encyclopedia of genes and genomes (KEGG) enrichment analysis showed that sphingolipid metabolism was significantly activated (Fig. 2a). According to the modified Pfirrmann grades [37,39], IVDD is divided into eight separate grades. Based on this system, CEPs corresponding to IVDD were also divided into eight grades. Immunohistochemistry and immunofluorescence staining showed that the expression of Sphk2 in the CEP increased significantly with the progression of IVDD (Fig. 2b). WB and RT-qPCR results showed that the Sphk2 protein and *Sphk2* mRNA levels increased in conjunction with the CEP grade (Fig. 2c and d). Moreover, the Sphk2 protein and *Sphk2* mRNA levels, which represent transcription and translation, respectively, were highly correlated in CEP ($R^2 = 0.93$) (Fig. 2e). The results also demonstrate that the expression of Sphk2 in the CEP increased significantly with the progression of IVDD.To further validate these results, an IVDD rat model was established. We measured Sphk2 protein levels using WB analysis, immunohistochemistry, and immunofluorescence analysis. These results indicate that the Sphk2 immunochemistry fluorescence intensity, as well as protein level, were notably increased in the NP area of IVDD rats when compared to the control group (Fig. 2f and g). This suggests that Sphk2 might enhance both the inhibition of cell senescence and IVDD by increasing expression level during IVDD progression.

To determine the difference in Sphk2 expression between degenerated (24 months) and normal (3 months) rat IVDs, the gene chip results were analyzed (**GSE126883**, https://www.ncbi.nlm.nih.gov/). The resulting heat map showed that Sphk2 expression was significantly higher in the IVDD group than in the normal control group (Fig. 2h). Clinical patient samples were graded using a modified Pfirrmann scale (Supplementary Figure 2), and *Sphk2* mRNA and Sphk2 protein expression increased with the increasing clinical IVDD degeneration grade (Fig. 2i–k). Correlation analysis showed that the correlation between the *Sphk2* mRNA and Sphk2 protein levels were also poor ($R^2 = 0.46$) (Figure 2l). The increased expression of Sphk2 in degenerated NP tissue was also verified in rat tissue (Fig. 2m–n). Immunofluorescence staining and WB analysis of normal IVDs showed that the Sphk2 protein expression in the CEP was higher than that in the NP area (Fig. 2o–p). The difference was even more pronounced in the degenerated rat IVD group (Figure 2q). These results suggest that CESCs produce more Sphk2 than NPCs, which may inhibit NPCs senescence and IVDD progression via transporting Sphk2 into the IVD.

Based on the above results and the fact that exosomes could be used as transport vehicles for a variety of proteins, we postulated that CESCs inhibit IVDD by releasing exosomes that transport Sphk2 into NPCs, thereby regulating disc degeneration progression. Therefore, we then measured the levels of Sphk2 in exosomes and CESCs using WB analysis. Consistent with the above hypotheses, the levels of Sphk2 in exosomes were significantly higher than in CESCs (Figure 2r). Moreover, after TBHP treatment, the expression of Sphk2 in both CESCs and secreted exosomes also increased significantly (Fig. 2s and t). To determine whether exosomes can transport Sphk2 into NPCs, the NPCs were pre-treated with PKH67-labeled exosomes. This determined that although a small amount of Sphk2 can be secreted by NPCs themselves, a larger amount of Sphk2 was transported into the cells by exosomes (Figure 2u).

3.3. Cartilage endplate stem cells -derived exosomes balance autophagy and senescence through the Sphk2/AKT pathway to inhibit intervertebral disc degeneration

Double immunofluorescence staining of exosomes and Sphk2 further supports the possibility that CESCs regulate disc degeneration by secreting exosomes transporting Sphk2 into the IVD (Supplementary Fig. 3). To explore whether the anti-senescence effect of exosomes is related to transporting Sphk2 into NPCs, we treated different experimental groups with TBHP, exosomes, and the Sphk2 inhibitor ABC294640. We found that exosomes inhibited cell senescence; however, this inhibitory effect was nullified by ABC294640 (Supplementary Fig. 4a). Additionally, exosomes significantly prevented the TBHP-induced increase in SA-β-gal activity, however, ABC294640 attenuated the exosome-mediated inhibition of SA-β-gal activity (Supplementary Fig. 4b). Therefore, we extracted the engineered exosomes produced by Lenti-*Sphk2*-and Lenti-sh*Sphk2*-transfected CESCs (Lenti-Sphk2-Exo and Lenti-shSphk2-Exo) to investigate the anti-aging mechanisms of exosomes and Sphk2 in NPCs. The preparation process is shown in Fig. 3a. Compared with Sphk2 expression in the Lenti–NC–transfected CESCs and Lenti–NC–Exo groups, Sphk2 expression in Lenti-*Sphk2*-transfected CESCs and Lenti-Sphk2-exosomes were significantly increased (Supplementary Fig. 5). We then examined three different types of exosomes for their anti-aging effects in NPCs by β-Gal staining and immunofluorescence staining for P16 and P21. Lenti-Sphk2-Exos had a significant anti-aging effect on NPCs (Supplementary Figs. 6a–b). The same phenomenon was also observed by WB analysis, wherein the Lenti-Sphk2-Exos

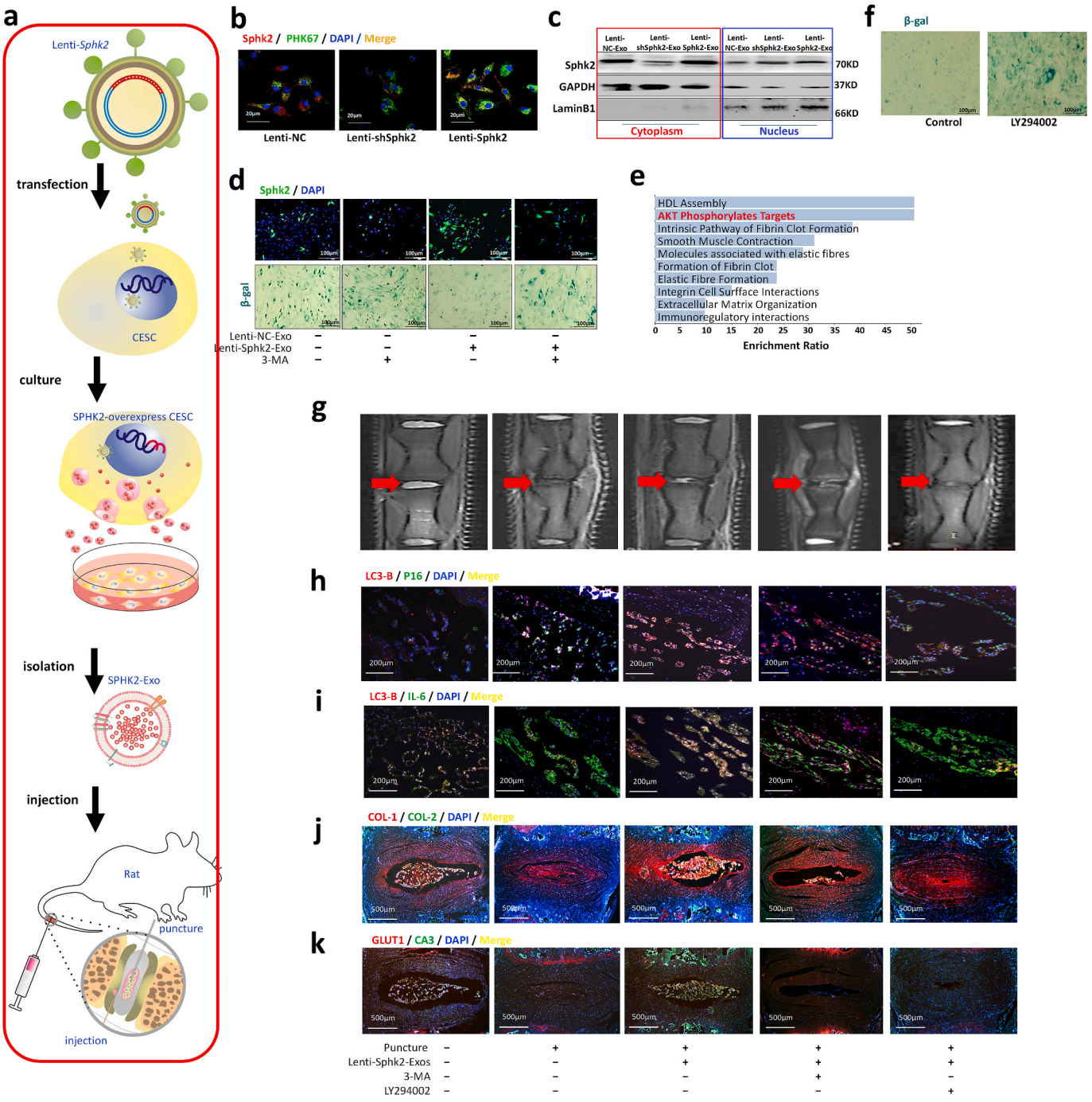

Fig. 3. Sphk2 located in the cytoplasm inhibits the progression of the senescence-associated secretory phenotype of nucleus pulposus cells to ameliorate intervertebral disc degeneration via activating the AKT/autophagy pathway

a) The diagram of engineered exosome acquisition and treatment of intervertebral disc degeneration. b) Double immunofluorescence of Sphk2 (red) and exosomes (green) in the nucleus or cytoplasm in the nucleus pulposus cells (NPCs) treated with Lenti–NC–exosome, Lenti-sh*Sphk2*-exosome and Lenti-Sphk2-exosome. c) Western blots and quantitative protein levels of Sphk2 in the nucleus or cytoplasm of NPCs when treated as above. d) Representative images of senescence-associated β-galactosidase (SA-β-Gal) staining and immunofluorescence staining were taken to detect senescence of NPCs treated with Lenti–NC–exosome, Lenti-sh*Sphk2*-exosome, Lenti-Sphk2-exosome, and Lenti-Sphk2-exosome + 3-MA. e) Bioinformatics enrichment analysis in rat intervertebral disc tissues. f) Immunofluorescence and SA-β-gal staining was used to detect the senescence of NPCs treated with the PI3K/AKT inhibitor LY294002. g) Representative magnetic resonance images of rat intervertebral discs treated by NC, puncture, puncture + lenti-Sphk2-exosome, puncture + lenti-Sphk2-exosome + 3-MA and puncture + lenti-Sphk2-exosome + LY294002. h-k) Double immunofluorescence of LC3B (red) and P16 (green) (h), LC3B (red) and IL-6 (green) (i), COL-1(red) and COL-2 (green) (j) or GLUT1(red) and CA3 (green) (k) in the above rat disc.

increased the ratio of the autophagy protein LC3B/A and decreased the expression of P16 and P21. However, this effect was reversed by Lenti-shSphk2-Exos (Supplementary Fig. 6c). In conclusion, the effect of CESC exosomes on apoptosis and aging inhibition in NPCs is mediated by the Sphk2 protein.

Correlation analysis of the genes associated with degeneration indicated that Sphk2 is positively related to the autophagy-associated protein ATG4C and negatively correlated with the cycle-related

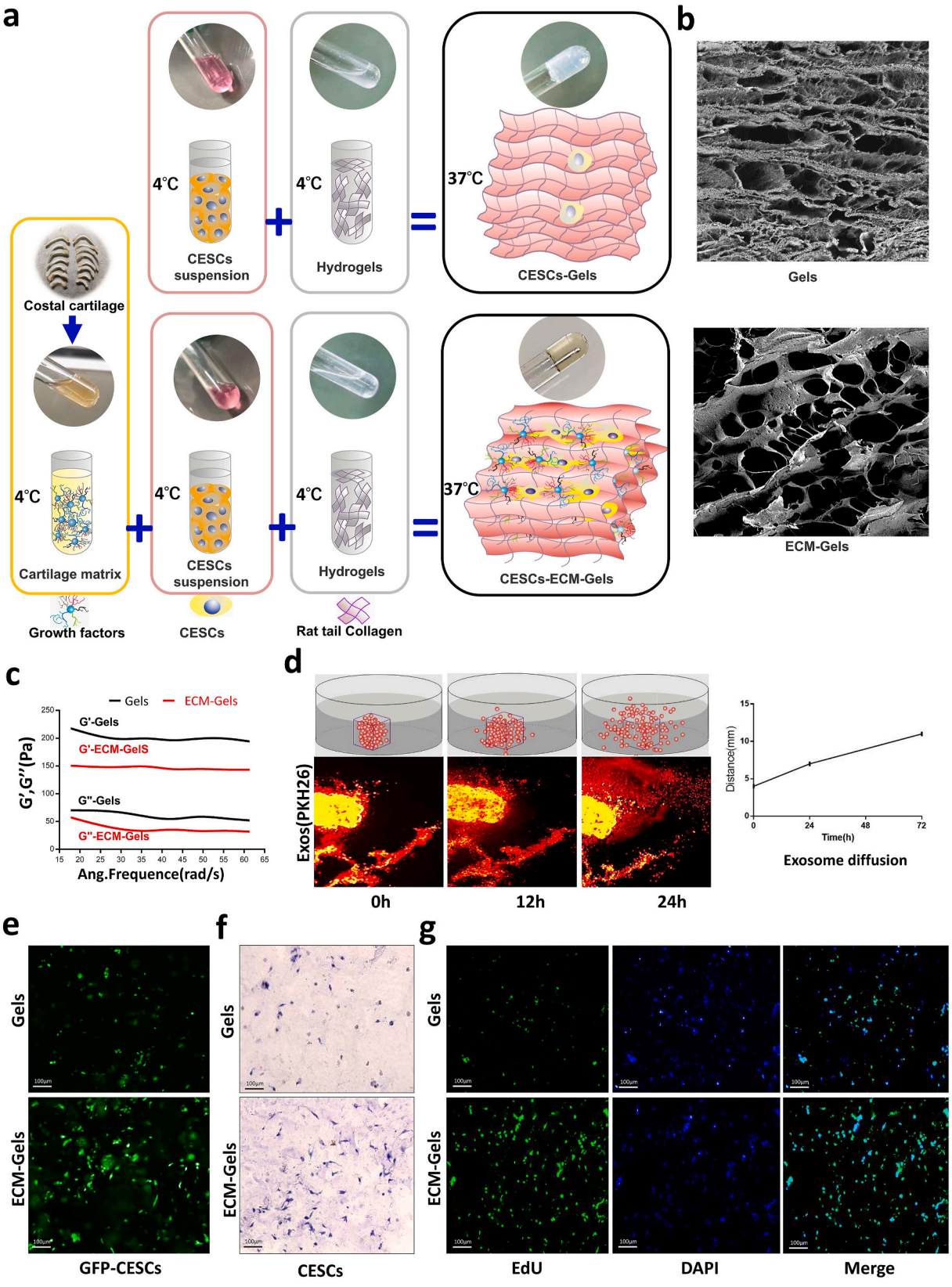

Fig. 4. Hydrogels modified with the extracellular matrix of costal cartilage promote cartilage endplate stem cell growth and proliferation and accelerate the spread of exosomes

a) Construction process of hydrogels (Gels) or hydrogels modified with the extracellular matrix of costal cartilage (ECM-Gels). b) Scanning electron microscope images of Gels or ECM-Gels. c) Analysis of storage modulus and loss modulus of Gels or ECM-Gels. d) PKH26-labeled exosomes gradually diffused into the hydrogel over time. e-g) Fluorescence intensity analysis, hematoxylin and eosin and EdU staining were used to detect the growth of cartilage endplate stem cells in Gels or ECM-Gels.

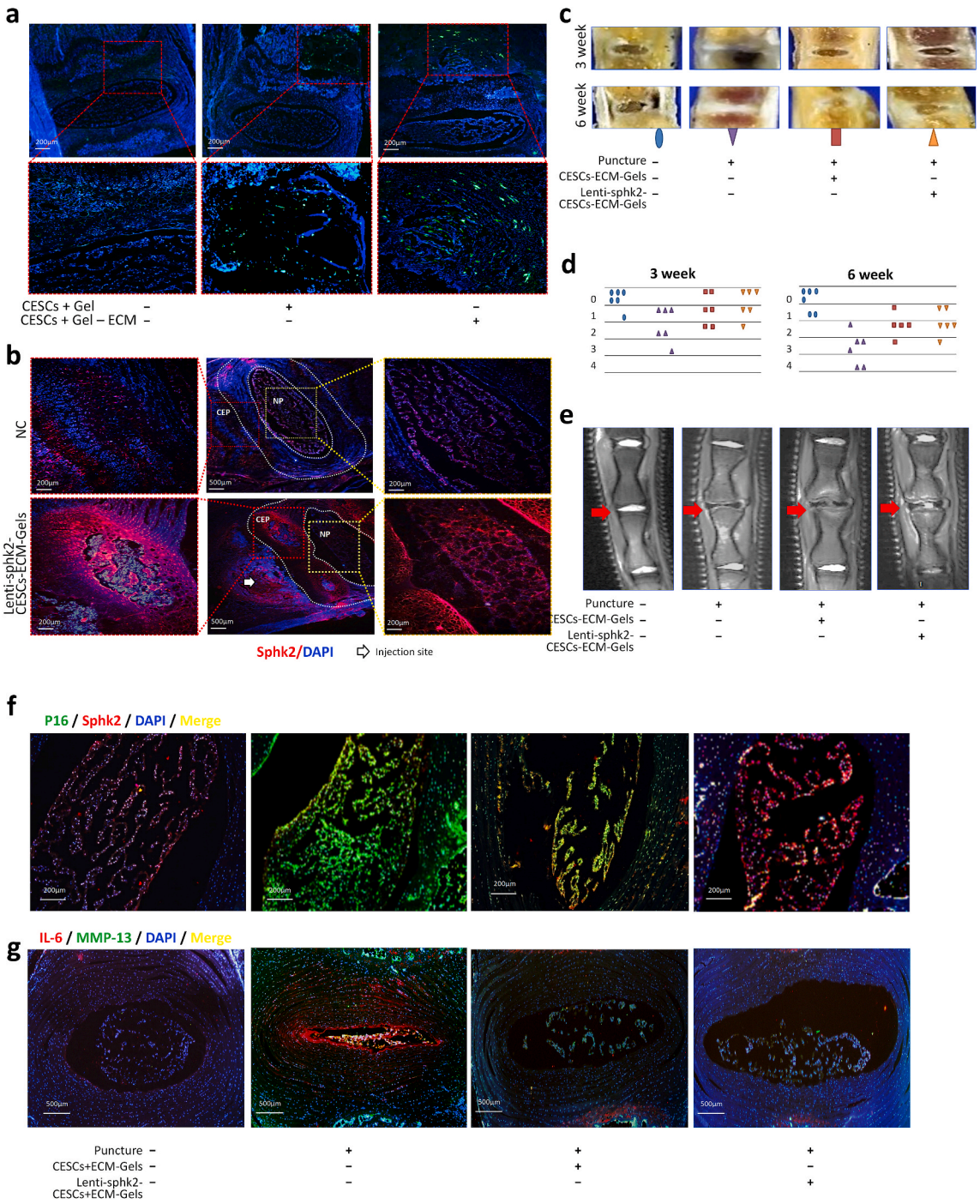

Fig. 5. Hydrogels modified with the extracellular matrix of costal cartilage loaded with Lenti-Sphk2-cartilage endplate stem cells release Lenti-Sphk2-exosomes into nucleus pulposus cells and inhibit intervertebral disc degeneration

a) Differences between ECM-Gels and Gels in promoting cell growth were analyzed by EGF-labeled CESCs in vivo. b) In normal IVD or IVD with ECM-Gel injection, the expression level of Sphk2 in both the ECM-Gels and CEP was detected. c-d) Morphology and metamorphosis score of intervertebral disc tissue at 3 and 6 weeks after treatment with either the normal control, puncture, puncture + CESCs-ECM-Gels and puncture + Lenti-Sphk2-CESCs-ECM-Gels. e-g) Magnetic resonance imaging, double immunofluorescence of Sphk2 (red) and P16 (green) or IL-6 (red) and MMP13 (green) in the above rat disc.

protein CDKN2A (P16) (GSE126883, https://www.ncbi.nlm.nih.gov/) (Supplementary Fig. 7). These results suggest that Sphk2 promotes NPC autophagy, thus inhibiting NPC senescence. The role of Sphk2 in activating autophagy and resisting senescence in rat NPCs were further clarified by extracting and identifying the high expression of collagen 2 and low expression of collagen 1in NPCs (Supplementary Fig. 8a). Sphk2 was then downregulated (Lenti-sh*Sphk2*) or overexpressed (Lenti-*Sphk2*) via the lentivirus vector. After constructing Lenti-*Sphk2*-transfected NPCs, we noticed that Sphk2 protein and *Sphk2* mRNA expression increased significantly, however, P16 expression decreased significantly. Additionally, the SA-β-gal staining assay demonstrated that the number of senescent NPCs decreased (Supplementary Figs. 8b–d). However, in Lenti-sh*Sphk2*-transfected cells, the opposite effect was observed (Supplementary Figs. 8e–g). TEM observation confirmed that the number of autophagosomes increased significantly in Lenti-*Sphk2*-transfected NPCs (Supplementary Fig. 9a). Furthermore, we found that

the LC3B/A ratio and level of the autophagy-associated protein Beclin-1 increased in the Lenti-*Sphk2*-transfected NPCs (Supplementary Fig. 9b). Moreover, immunofluorescence staining showed that the autophagosome fluorescence intensity increased in Lenti-*Sphk2*-transfected cells (Supplementary Fig. 9c). Thus, we then added the autophagy promoter rapamycin, and inhibitor 3-MA to the NPCs. We identified that expression of P16 and P21 decreased after autophagic flux was increased, and as expected they increased after autophagic flux was decreased (Supplementary Fig. 9d). Immunofluorescence staining, SA-β-gal staining, and WB analysis revealed that the senescence proteins were significantly downregulated in Lenti-*Sphk2*-transfected NPCs (Supplementary Figs. 9e–f). Taken together, these results indicate that Sphk2 overexpression enhances autophagic flux and inhibits NPC senescence.

Previous studies have shown that Sphk2-mediated senescence regulation in different cells may induce the opposite effects, this is closely related to its expression in the cytoplasm or nucleus. Lenti–NC–Exos, Lenti-shSphk2-Exos, and Lenti-Sphk2-Exos were labeled with PKH67 and added to NPCs. Immunofluorescence staining indicated that Lenti-Sphk2-Exos transported more Sphk2 than other exosomes, furthermore it confirmed that Sphk2 was mainly expressed in the cytoplasm (Fig. 3b). Next, cytoplasmic and nuclear fractions were isolated, and WB analysis was performed. The results showed that the level of Sphk2 in the cytoplasm was significantly higher than in the nucleus in NPCs treated with all three exosomes (Fig. 3c). Different groups were then treated with engineered Lenti-Sphk2-Exos alongside the autophagy inhibitor 3-MA to confirm whether exosome-transported Sphk2 could mediate NPC aging inhibition, and whether this is related to autophagy. Immunofluorescence and SA-β-gal staining showed that the number of senescent cells decreased (Fig. 3d).

The WB results showed that the engineered Lenti-Sphk2-Exos significantly inhibited the expression of SASP proteins, such as MMP1, IL-6, IL-1, as well as the senescence proteins P16 and P21, however, this effect was reversed in the presence of 3-MA (Supplementary Fig. 10a). Based on the bioinformatics results, there was a significant difference in the activation of the AKT signaling pathway between degenerated and normal discs (GSE126883, https://www.ncbi.nlm.nih.gov/) (Fig. 3e). Thus, we treated NPCs with Lenti-*Sphk2* or the Sphk2 inhibitor ABC294640. We determined that the p-AKT signaling pathway was activated after Sphk2 overexpression, however, upon adding inhibitors, the p-AKT signaling pathway was effectively suppressed. We then examined other signaling pathways, such as p–NF–κB and p-JNK, however, no significant changes were demonstrated (Supplementary Fig. 10b). Moreover, we found that the ratio of the autophagy protein LC3B/A increased while the expression of P16, P21, and SASP proteins decreased significantly after the activation of the p-AKT signaling pathway. This effect was successfully inhibited by the AKT inhibitor LY294002 (Supplementary Fig. 10c). SA-β-gal staining in the experimental group indicated that NPC senescence increased markedly in the presence of LY294002 when compared to the control group (Fig. 3 f). These results suggest that exosomes can transport Sphk2 which activates the cytoplasmic AKT pathway, thus enhancing autophagy and inhibiting senescence of NPCs.

Subsequently, we extracted Lenti-*Sphk2* exosomes and Lenti-sh*Sphk2* exosomes and injected them into rat caudal IVDs. The following LC3B and Sphk2 double fluorescent staining of the frozen sections showed that the expression of LC3B increased with increasing Sphk2 expression, however, when Sphk2 expression decreased so too did LC3B (Supplementary Fig. 11). The rats were divided into five groups: NC, puncture, puncture + lenti-Sphk2-exosome, puncture + lenti-Sphk2-exosome + 3-MA, and puncture + lenti-Sphk2-exosome + LY294002. MRI results suggested that punctures, LY294002 and 3-MA exacerbated the degeneration of IVDs, whereas exosomes alleviated disc degeneration (Fig. 3g). The immunofluorescence staining results also showed that exosomes inhibited the puncture-induced expression of P16 and IL-6 via increasing LC3B expression, whereas 3-MA and LY294002 increased the puncture-induced expression of P16 (Fig. 3h and i). we also found that the expression of COL-1, GLUT1 and CA3 increased with an decrease in COL-2 expression (Fig. 3j and k). In short, we demonstrated that exosomes can inhibit the senescence of NPCs repair the IVDD by activating autophagy via the Sphk2/PI3K/AKT signaling pathway in vivo.

3.4. Extracellular matrix of costal cartilage hydrogels provide a suitable microenvironment for the growth and proliferation of cartilage endplate stem cells and the spread of exosomes

The cartilage extracellular matrix contains cytokines that promote CESC growth and proliferation; therefore, we constructed rat tail collagen hydrogels (Gels) as well as ECM-Gels to verify the effect of ECM-Gels on cell proliferation and growth. The construction process of ECM-Gels is shown in Fig. 4a, moreover, scanning electron microscopy results showed that ECM-Gels had larger pores (Fig. 4b). By introducing ECM components, the G′ and G″ of ECM-Gels were lower than those of the control group, indicating that the ECM-Gels were loose and porous, with weak mechanical strength (Fig. 4c). We also found that PKH26-labeled exosomes gradually diffused into the hydrogel over time. After 24 h of injection in the hydrogel, exosomes can spread out approximately 10 mm (Fig. 4d). After the inoculation of GFP-labeled CESCs into the hydrogels, we discovered that CESCs grew better in ECM-Gels (Fig. 4e). Using HE and EdU staining, we found that CESCs in ECM-Gels had higher growth and proliferation rates (Fig. 4f and g). Therefore, the results indicated that ECM-Gels were more conducive to the proliferation and growth of CESCs.

3.5. Cartilage extracellular matrix modified hydrogels loaded with Lenti-Sphk2-CESCs alleviate intervertebral disc degeneration long-term and stably via releasing Lenti-Sphk2-Exos

Injectable hydrogels provide the skeleton structure and sites required for cell proliferation and growth. Therefore, injectable ECM-Gels were used to construct Lenti-Sphk2 engineered CESC sites near to the cartilage endplate. In the in vivo experiments, we found that ECM-Gels were more beneficial to cell growth because we observed cell morphological changes (Fig. 5a). In normal IVD, the expression levels of Sphk2 in both the CEP and NP did not change significantly. However, in IVD with ECM-Gel injection, the expression levels of Sphk2 in both the ECM-Gels and CEP was not only higher than that in the NP tissue, but it was also significantly increased compared with normal IVD. This shows that the expression of Sphk2 in IVD was significantly increased after injecting ECM-Gels loaded with Lenti-*Sphk2* engineered CESCs. Moreover Sphk2 could migrate from the hydrogel injection site or cartilage endplate to the NP (Fig. 5b). To verify that Lenti-*Sphk2* engineered CESCs (Lenti-*Sphk2*-CESCs) can continuously produce engineered exosomes to inhibit IVDD, in a superior way to just CESCs, we divided the rats into four groups: NC, puncture, puncture + ECM-Gels loaded with CESCs, and puncture + ECM-Gels loaded with Lenti-Sphk2-CESCs. Rat IVDs were obtained at 6 weeks. Disc degeneration was observed in longitudinal sections, and we discovered that IVDD could be repaired by ECM-Gels loaded with Lenti-*Sphk2*-CESCs; these were more effective than ECM-Gels loaded with normal CESCs (Fig. 5c). The statistical analysis of the degree of damage in the AF and the height of the IVD (Supplementary Table 1) are shown in Fig. 5d. Furthermore, MRI results suggest that ECM-Gels loaded with Lenti-*Sphk2*-CESCs alleviated disc degeneration more effectively than ECM-Gels loaded with CESCs (Fig. 5e). Immunofluorescence staining also confirmed that ECM-Gels loaded with Lenti-*Sphk2*-CESCs could release exosomes carrying more Sphk2 into NPCs thereby inhibiting the expression of P16, IL-6 and MMP13, which inhibits the degeneration of intervertebral discs (Fig. 5f and g).

4. Discussion

Most people will suffer or are suffering from lower back pain, mainly caused by IVDD, which involves the interaction of multiple immune and

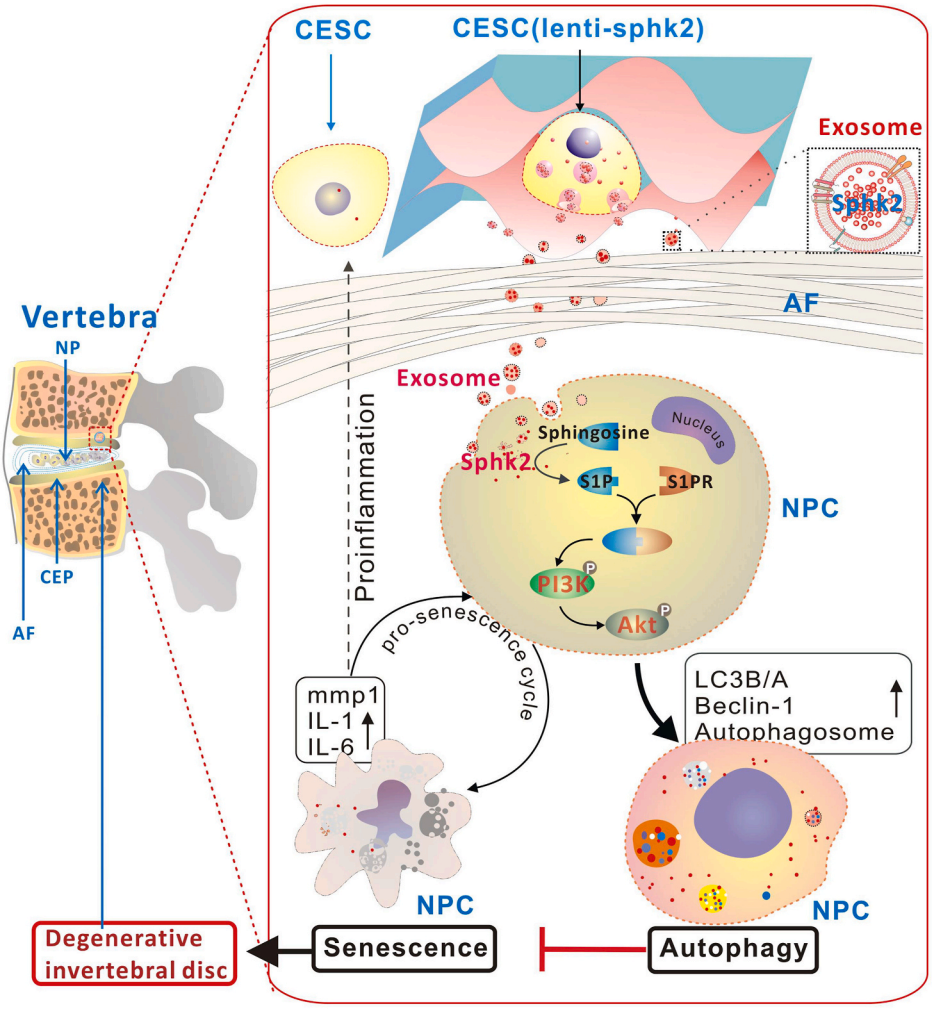

Fig. 6. Graphical abstract
Hydrogels modified with the extracellular matrix of costal cartilage (ECM-Gels) loaded with Lenti-Sphk2-cartilage endplate stem cells (CESCs) near the cartilage endplate (CEP) produced Lenti-Sphk2-exosomes (Exos) continuously and steadily. Lenti-Sphk2-Exos could cut across the annulus fibrous and carry Sphk2 into nucleus pulposus cells (NPCs). After entering the cytoplasm, Sphk2 phosphorylates sphingosine and generates sphingosine-1-phosphate (S1P), thus activating the intracellular PI3K/AKT signaling pathway and increasing autophagy. Activation of autophagy could inhibit senescence of NPCs by reducing SASP protein expression. Ultimately, Lenti-Sphk2-Exos ameliorated intervertebral disc degeneration by balancing autophagy/senescence.

biological systems [24]. Although invasive surgery can partially ameliorate the disease, there are risks of surgical injury and worsening of immune-mediated tissue damage [40]. Hence, non-surgical treatment and prevention can represent more attractive strategies [41]. The herein described engineered hydrogel is injected near the endplate of the cartilage without destroying the AF and NP. The solidified hydrogel will then slowly release the impregnated Lenti-Sphk2-exosomes to the NP region throughout time, thereby avoiding the double damage of surgery and immunity and inhibiting IVDD progress. This highlights the positive significance of our research.

Hydrogel has been widely used in three-dimensional cell culture, experiments, and clinical investigations [42,43], as it can provide a microenvironment that favors the survival of engineered cells [44]. Furthermore, cytokine-modified hydrogels maintain cell activity more effectively [45,46]. We found that the costal cartilage extracellular matrix acts as positive factor, maintaining CESCs alive and in good shape. Moreover, ECM-Gels significantly promoted CESC proliferation and growth *in vitro* and in vivo, and provided suitable support for the continuous release of exosomes from engineered CESCs. Hydrogels loaded with exosomes can be used therapeutic tools for the treatment of various diseases [47,48]. However, the limited number of exosomes that could be placed in hydrogels and the inability to sustain long-term stable release of exosomes are some pitfalls of this approach. Therefore, the construction of engineering cells with continuous release of exosomes, along with a hydrogel that enables their growth, is of great significance. We studied the effect of hydrogels carrying Lenti-Sphk2-CESCs on IVDD in vivo. ECM-Gels loaded with Lenti-Sphk2-CESCs were found to produce sufficient and functional Sphk2, which was then transported by exosomes into the NP tissue in a rat model of IVD. These results demonstrate the obvious advantage of this new therapeutic strategy for IVDD treatment.

Exosomes are extracellular vesicles that transport active cellular components, such as proteins, and DNA and RNA molecules, between cells and represent a good possibility as drug delivery system. Therefore, they have attracted increasing attention as therapeutic tools for degenerative diseases [49,50]. MSC-derived exosomes improve disc degeneration through antioxidant and anti-inflammatory effects [51], as well as by reducing endoplasmic reticulum stress in NPCs [14]. However, given that the intervertebral disc is an immune privileged organ, autologous CESCs are more suitable for implantation in the intervertebral disc as treatment for IVDD. Our previous study confirmed that exosomes from CESCs are involved in IVDD [52]. However, the specific cellular and molecular mechanism is unclear. NPCs play a key role in the generation and maintenance of extracellular matrix, and IVDD is aggravated by decrease of NPCs and degeneration of extracellular. IVDD is also characterized by senescence and apoptosis of NPCs [53]. CESCs, AF stem cells, chondrocytes, and exosomes were all found to have a significant effect during repair of IVDD [54].· [55] Numerous studies have also shown that stem cells can produce exosomes that inhibit cell senescence [56,57]. We discovered that CESC-Exos can improve puncture-induced IVDD, and confirmed that Sphk2 plays an important role in this process. A study has shown that exosomes derived from liver cells can carry Sphk2 to repair damaged liver tissue [13]. Herein, we determined that CESC-Exos could be used to carry Sphk2 into the NPCs, thus inhibiting

IVDD in rats. Sphk2 is a natural protein that can shuttle freely between the CEP and the NP through the exosome pathway. Hence, Sphk2 holds great therapeutic potential for IVD, and is the core of our engineered exosomes.

Recent studies have shown that the effect of Sphk2 on cell senescence is mainly dependent on its localization within the cells. Sphk2 is mainly expressed in the cytoplasm and can inhibit aging and promote proliferation [58], but it can also be expressed in the nucleus where it promotes cell growth inhibition [35,59]. Research shows that decreased expression of Sphk2 in fibroblasts and tumor cells reduced cell proliferation and increased markers of senescence [60,61]. Through the activation of autophagy, Sphk2 could delay aging, but the specific signaling pathway was not clear. Autophagy is a highly conserved catabolic process, which is involved in a variety of cellular biological activities. AKT pathway is considered as a critical autophagy regulator and involved in the initiation and promotion of various pathological disorders [61–63]. In a previous study, authors demonstrated that artesunate accelerated autophagy in rheumatoid arthritis rats through the PI3K/AKT/mTOR signaling pathway [64]. Moreover, another study has proved that PI3K/AKT/mTOR-mediated autophagy played a key role in development of autism spectrum disorder [65]. Thus, the role of PI3K/AKT/mTOR pathway in the modulation of autophagy is important. After PKH67-labeled exosomes were transferred into NPCs, we found that Sphk2 was mainly expressed in the cytoplasm and inhibited NPC senescence. Moreover, the effects of Lenti-Sphk2-Exos on inhibiting NPC senescence and disc degeneration were noticeably weakened after adding either an mTOR or AKT pathway inhibitors *in vitro* or in vivo [66]. These results indicate that Lenti-Sphk2-Exos can enter NPCs to inhibit disc degeneration by releasing Sphk2 and enhancing autophagy through the activation of the PI3K/AKT signaling pathway.

5. Conclusions

In summary, this work demonstrates that ECM-Gels encapsulating Lenti-Sphk2-CESCs continuously and stably release exosomes that can pass through the AF and transport Sphk2 into NPCs when situated near the CEP. Furthermore, Lenti-Sphk2-Exos can regulate the autophagy/senescence of NPCs and prevent disc degeneration through the activation of the PI3K/AKT signaling pathway both *in vitro* and in vivo (Fig. 6). These results not only provide further support for CESC-Exos and Sphk2 as potential therapeutic tools for IVDD prevention, but they also provide a theoretical basis for IVDD treatment using continuous release of Sphk2-loaded engineered exosomes near the CEP.

CRediT authorship contribution statement

Liwen Luo: Methodology, Validation, Investigation, Writing – original draft, preparation, Writing – review & editing. **Junfeng Gong:** Investigation, Writing – review & editing. Zhouguang Wang: Methodology, Validation, Formal analysis, Writing – review & editing. **Yao Liu:** Methodology, Investigation, Validation, Formal analysis. **Jiaming Cao:** Resources, Writing – review & editing. **Jinghao Qin:** Methodology, Validation, Investigation. **Rui Zuo:** Writing – review & editing. **Hongyu Zhang:** Resources, Writing – review & editing. Shuai Wang: Writing – review & editing. **Ping Zhao:** Formal analysis, Writing – original draft, preparation. **Di Yang:** Writing – review & editing. **Mengjie Zhang:** Project administration, Writing – review & editing. **Yanqiu Wang:** Project administration, Writing – review & editing. **Junfeng Zhang:** Writing – review & editing. **Yue Zhou:** Conceptualization, Funding acquisition. **Changqing Li:** Project administration, Writing – review & editing. **Bing Ni:** Project administration, Writing – review & editing. **Zhiqiang Tian:** Conceptualization, Funding acquisition, Writing – review & editing. **Minghan Liu:** Conceptualization, Funding acquisition, Writing – review & editing.

Declaration of competing interest

All the authors declare that they have no conflict of interest.

Acknowledgments

This work was supported by the National Natural Science Foundation of China (Grant Number: 81874028, 81702182); the Research Program of Foundation Science and Application Technology of Chongqing (Grant Number: cstc2018jcyjAX0598) and Basic Medical College Foundation of Army Medical University (2019JCZX10).

Appendix A. Supplementary data

Supplementary data to this article can be found online at https://doi.org/10.1016/j.bioactmat.2021.12.007.

References

[1] L. Manchikanti, V. Singh, F.J. Falco, R.M. Benyamin, J.A. Hirsch, Epidemiology of low back pain in adults, Neuromodulation : journal of the International Neuromodulation Society (2014) 3–10.
[2] F.J. Lyu, K.M. Cheung, Z. Zheng, H. Wang, D. Sakai, V.Y. Leung, IVD progenitor cells: a new horizon for understanding disc homeostasis and repair, Nat. Rev. Rheumatol. 15 (2) (2019) 102–112.
[3] A. Dunn, S.D. Grosse, S.H. Zuvekas, Adjusting health expenditures for inflation: a review of measures for health services research in the United States, Health Serv. Res. 53 (1) (2018) 175–196.
[4] F. Collino, M. Pomatto, S. Bruno, R.S. Lindoso, M. Tapparo, W. Sicheng, P. Quesenberry, G. Camussi, Exosome and microvesicle-enriched fractions isolated from mesenchymal stem cells by gradient separation showed different molecular signatures and functions on renal tubular epithelial cells, STEM CELL REV REP 13 (2) (2017) 226–243.
[5] R.C. Lai, S.S. Tan, B.J. Teh, S.K. Sze, F. Arslan, D.P. de Kleijn, A. Choo, S.K. Lim, Proteolytic potential of the MSC exosome proteome: implications for an exosome-mediated delivery of therapeutic proteasome, International journal of proteomics 2012 (2012) 971907.
[6] X. Liu, Y. Yang, Y. Li, X. Niu, B. Zhao, Y. Wang, C. Bao, Z. Xie, Q. Lin, L. Zhu, Integration of stem cell-derived exosomes with in situ hydrogel glue as a promising tissue patch for articular cartilage regeneration, Nanoscale 9 (13) (2017) 4430–4438.
[7] G. Liang, Y. Zhu, D.J. Ali, T. Tian, H. Xu, K. Si, B. Sun, B. Chen, Z. Xiao, Engineered exosomes for targeted co-delivery of miR-21 inhibitor and chemotherapeutics to reverse drug resistance in colon cancer, J. Nanobiotechnol. 18 (1) (2020) 10.
[8] H. Nojima, C.M. Freeman, R.M. Schuster, L. Japtok, B. Kleuser, M.J. Edwards, E. Gulbins, A.B. Lentsch, Hepatocyte exosomes mediate liver repair and regeneration via sphingosine-1-phosphate, J. Hepatol. 64 (1) (2016) 60–68.
[9] X.F. Gao, Z.M. Wang, F. Wang, Y. Gu, J.J. Zhang, S.L. Chen, Exosomes in coronary artery disease, Int. J. Biol. Sci. 15 (11) (2019) 2461–2470.
[10] X. Huang, J. Ding, Y. Li, W. Liu, J. Ji, H. Wang, X. Wang, Exosomes derived from PEDF modified adipose-derived mesenchymal stem cells ameliorate cerebral ischemia-reperfusion injury by regulation of autophagy and apoptosis, Exp. Cell Res. 371 (1) (2018) 269–277.
[11] J.H. Dominguez, Y. Liu, H. Gao, J.M. Dominguez, D. Xie, K.J. Kelly, Renal tubular cell-derived extracellular vesicles accelerate the recovery of established renal ischemia reperfusion injury, J. Am. Soc. Nephrol. : JASN (J. Am. Soc. Nephrol.) 28 (12) (2017) 3533–3544.
[12] W. Minghua, G. Zhijian, H. Chahua, L. Qiang, X. Minxuan, W. Luqiao, Z. Weifang, L. Peng, Z. Biming, Y. Lingling, W. Zhenzhen, X. Jianqing, B. Huihui, W. Xiaozhong, C. Xiaoshu, Plasma exosomes induced by remote ischaemic preconditioning attenuate myocardial ischaemia/reperfusion injury by transferring miR-24, Cell Death Dis. 9 (3) (2018) 320.
[13] H. Nojima, C.M. Freeman, R.M. Schuster, L. Japtok, B. Kleuser, M.J. Edwards, E. Gulbins, A.B. Lentsch, Hepatocyte exosomes mediate liver repair and regeneration via sphingosine-1-phosphate, J. Hepatol. 64 (1) (2016) 60–68.
[14] Z. Liao, R. Luo, G. Li, Y. Song, S. Zhan, K. Zhao, W. Hua, Y. Zhang, X. Wu, C. Yang, Exosomes from mesenchymal stem cells modulate endoplasmic reticulum stress to protect against nucleus pulposus cell death and ameliorate intervertebral disc degeneration in vivo, THERANOSTICS 9 (14) (2019) 4084–4100.
[15] Y. Che, X. Shi, Y. Shi, X. Jiang, Q. Ai, Y. Shi, F. Gong, W. Jiang, Exosomes derived from miR-143-overexpressing MSCs inhibit cell migration and invasion in human prostate cancer by downregulating TFF3. Molecular therapy, Nucleic acids 18 (2019) 232–244.
[16] G. Xu, B. Zhang, J. Ye, S. Cao, J. Shi, Y. Zhao, Y. Wang, J. Sang, Y. Yao, W. Guan, J. Tao, M. Feng, W. Zhang, Exosomal miRNA-139 in cancer-associated fibroblasts inhibits gastric cancer progression by repressing MMP11 expression, Int. J. Biol. Sci. 15 (11) (2019) 2320–2329.
[17] L. Yu, S. Gui, Y. Liu, X. Qiu, G. Zhang, X. Zhang, J. Pan, J. Fan, S. Qi, B. Qiu, Exosomes derived from microRNA-199a-overexpressing mesenchymal stem cells

inhibit glioma progression by down-regulating AGAP2, Aging 11 (15) (2019) 5300–5318.
[18] X. Xu, Y. Liang, X. Li, K. Ouyang, M. Wang, T. Cao, W. Li, J. Liu, J. Xiong, B. Li, J. Xia, D. Wang, L. Duan, Exosome-mediated delivery of kartogenin for chondrogenesis of synovial fluid-derived mesenchymal stem cells and cartilage regeneration, Biomaterials (2020) 120539.
[19] G. Liang, S. Kan, Y. Zhu, S. Feng, W. Feng, S. Gao, Engineered exosome-mediated delivery of functionally active miR-26a and its enhanced suppression effect in HepG2 cells, Int. J. Nanomed. 13 (2018) 585–599.
[20] K. Zhang, X. Zhao, X. Chen, Y. Wei, W. Du, Y. Wang, L. Liu, W. Zhao, Z. Han, D. Kong, Q. Zhao, Z. Guo, Z. Han, N. Liu, F. Ma, Z. Li, Enhanced therapeutic effects of mesenchymal stem cell-derived exosomes with an injectable hydrogel for hindlimb ischemia treatment, ACS APPL MATER INTER 10 (36) (2018) 30081–30091.
[21] T.H. Qazi, D.J. Mooney, G.N. Duda, S. Geissler, Biomaterials that promote cell-cell interactions enhance the paracrine function of MSCs, Biomaterials 140 (2017) 103–114.
[22] B. Borde, P. Grunert, R. Härtl, L.J. Bonassar, Injectable, high-density collagen gels for annulus fibrosus repair: an in vitro rat tail model, J. Biomed. Mater. Res. 103 (8) (2015) 2571–2581.
[23] M.A. Jafri, G. Kalamegam, M. Abbas, M. Al-Kaff, F. Ahmed, S. Bakhashab, M. Rasool, M.I. Naseer, V. Sinnadurai, P.N. Pushparaj, Ex vivoDeciphering the association of cytokines, chemokines, and growth factors in chondrogenic differentiation of human bone marrow mesenchymal stem cells using an osteochondral culture system, Front. Cell Dev. Biol. 7 (2019) 380.
[24] Z. Sun, B. Liu, Z.J. Luo, The immune privilege of the intervertebral disc: implications for intervertebral disc degeneration treatment, Int. J. Med. Sci. 17 (5) (2020) 685–692.
[25] Z. Li, X. Wang, H. Pan, H. Yang, X. Li, K. Zhang, H. Wang, Z. Zheng, H. Liu, J. Wang, Resistin promotes CCL4 expression through toll-like receptor-4 and activation of the p38-MAPK and NF-κB signaling pathways: implications for intervertebral disc degeneration, OSTEOARTHR CARTILAGE 25 (2) (2017) 341–350.
[26] L. Luo, X. Jian, H. Sun, J. Qin, Y. Wang, J. Zhang, Z. Shen, D. Yang, C. Li, P. Zhao, M. Liu, Z. Tian, Y. Zhou, Cartilage endplate stem cells inhibit intervertebral disc degeneration by releasing exosomes to nucleus pulposus cells to activate Akt/autophagy, Stem cells 39 (4) (2021) 467–481.
[[27] C. Xu, W. Zhang, S. Liu, W. Wu, M. Qin, J. Huang, Activation of the SphK1/ERK/p-ERK pathway promotes autophagy in colon cancer cells, Oncol. Lett. 15 (6) (2018) 9719–9724.
[28] Y. Chen, X. Deng, W. Chen, P. Shi, M. Lian, H. Wang, K. Wang, D. Qian, D. Xiao, H. Long, Silencing of microRNA-708 promotes cell growth and epithelial-to-mesenchymal transition by activating the SPHK2/AKT/β-catenin pathway in glioma, Cell Death Dis. 10 (6) (2019) 448.
[29] D.D. Song, T.T. Zhang, J.L. Chen, Y.F. Xia, Z.H. Qin, C. Waeber, R. Sheng, Sphingosine kinase 2 activates autophagy and protects neurons against ischemic injury through interaction with Bcl-2 via its putative BH3 domain, Cell Death Dis. 8 (7) (2017), e2912.
[30] C. Kang, Q. Xu, T.D. Martin, M.Z. Li, M. Demaria, L. Aron, T. Lu, B.A. Yankner, J. Campisi, S.J. Elledge, The DNA damage response induces inflammation and senescence by inhibiting autophagy of GATA4, Science (New York, N.Y.) 349 (6255) (2015) a5612.
[31] B. Han, K. Zhu, F.C. Li, Y.X. Xiao, J. Feng, Z.L. Shi, M. Lin, J. Wang, Q.X. Chen, A simple disc degeneration model induced by percutaneous needle puncture in the rat tail, Spine 33 (18) (2008) 1925–1934.
[32] C. Théry, S. Amigorena, G. Raposo, A. Clayton, Isolation and characterization of exosomes from cell culture supernatants and biological fluids, Current protocols in cell biology (2006) 3–22.
[33] I. Campoy, L. Lanau, T. Altadill, T. Sequeiros, S. Cabrera, M. Cubo-Abert, A. Pérez-Benavente, A. Garcia, S. Borrós, A. Santamaria, J. Ponce, X. Matias-Guiu, J. Reventós, A. Gil-Moreno, M. Rigau, E. Colas, Exosome-like vesicles in uterine aspirates: a comparison of ultracentrifugation-based isolation protocols, J. Transl. Med. 14 (1) (2016) 180.
[34] A.E. Simões, D.M. Pereira, J.D. Amaral, A.F. Nunes, S.E. Gomes, P.M. Rodrigues, A. C. Lo, R. D'Hooge, C.J. Steer, S.N. Thibodeau, P.M. Borralho, C.M. Rodrigues, Efficient recovery of proteins from multiple source samples after TRIzol(®) or TRIzol(®)LS RNA extraction and long-term storage, BMC Genom. 14 (2013) 181.
[35] W. Xue, L. Zender, C. Miething, R.A. Dickins, E. Hernando, V. Krizhanovsky, C. Cordon-Cardo, S.W. Lowe, Senescence and tumour clearance is triggered by p53 restoration in murine liver carcinomas, Nature 445 (7128) (2007) 656–660.
[36] J. Chen, J.J. Xie, M.Y. Jin, Y.T. Gu, C.C. Wu, W.J. Guo, Y.Z. Yan, Z.J. Zhang, J. L. Wang, X.L. Zhang, Y. Lin, J.L. Sun, G.H. Zhu, X.Y. Wang, Y.S. Wu, Sirt6 overexpression suppresses senescence and apoptosis of nucleus pulposus cells by inducing autophagy in a model of intervertebral disc degeneration, Cell Death Dis. 9 (2) (2018) 56.
[37] Y.J. Che, J.B. Guo, T. Liang, X. Chen, W. Zhang, H.L. Yang, Z.P. Luo, Assessment of changes in the micro-nano environment of intervertebral disc degeneration based on Pfirrmann grade, Spine J. : official journal of the North American Spine Society 19 (7) (2019) 1242–1253.
[38] R. Zuo, Y. Wang, J. Li, J. Wu, W. Wang, B. Li, C. Sun, Z. Wang, C. Shi, Y. Zhou, M. Liu, C. Zhang, Rapamycin induced autophagy inhibits inflammation-mediated endplate degeneration by enhancing Nrf2/Keap1 signaling of cartilage endplate stem cells, Stem cells (Dayton, Ohio) 37 (6) (2019) 828–840.
[39] L.P. Yu, W.W. Qian, G.Y. Yin, Y.X. Ren, Z.Y. Hu, MRI assessment of lumbar intervertebral disc degeneration with lumbar degenerative disease using the Pfirrmann grading systems, PLoS One 7 (12) (2012), e48074.
[40] M.V. Risbud, I.M. Shapiro, Role of cytokines in intervertebral disc degeneration: pain and disc content, Nat. Rev. Rheumatol. 10 (1) (2014) 44–56.
[41] J.N. Weinstein, T.D. Tosteson, J.D. Lurie, A.N. Tosteson, B. Hanscom, J.S. Skinner, W.A. Abdu, A.S. Hilibrand, S.D. Boden, R.A. Deyo, Surgical vs nonoperative treatment for lumbar disk herniation: the Spine Patient Outcomes Research Trial (SPORT): a randomized trial, JAMA 296 (20) (2006) 2441–2450.
[42] N. Gjorevski, M.P. Lutolf, Synthesis and characterization of well-defined hydrogel matrices and their application to intestinal stem cell and organoid culture, Nat. Protoc. 12 (11) (2017) 2263–2274.
[43] Z. Li, S. Hu, K. Cheng, Chemical engineering of cell therapy for heart diseases, Accounts Chem. Res. 52 (6) (2019) 1687–1696.
[44] W.Y. Lee, Y.H. Chang, Y.C. Yeh, C.H. Chen, K.M. Lin, C.C. Huang, Y. Chang, H. W. Sung, The use of injectable spherically symmetric cell aggregates self-assembled in a thermo-responsive hydrogel for enhanced cell transplantation, Biomaterials 30 (29) (2009) 5505–5513.
[45] M. Samberg, R. Stone, S. Natesan, A. Kowalczewski, S. Becerra, N. Wrice, A. Cap, R. Christy, Platelet rich plasma hydrogels promote in vitro and in vivo angiogenic potential of adipose-derived stem cells, Acta Biomater. 87 (2019) 76–87.
[46] T. Böck, V. Schill, M. Krähnke, A.F. Steinert, J. Tessmar, T. Blunk, J. Groll, TGF-β1-Modified hyaluronic acid/poly(glycidol) hydrogels for chondrogenic differentiation of human mesenchymal stromal cells, Macromol. Biosci. 18 (7) (2018), e1700390.
[47] E.A. Mol, Z. Lei, M.T. Roefs, M.H. Bakker, M.J. Goumans, P.A. Doevendans, P. Dankers, P. Vader, J. Sluijter, Injectable supramolecular ureidopyrimidinone hydrogels provide sustained release of extracellular vesicle therapeutics, ADV HEALTHC MATER 8 (20) (2019), e1900847.
[48] N. Xu, L. Wang, J. Guan, C. Tang, N. He, W. Zhang, S. Fu, Wound healing effects of a Curcuma zedoaria polysaccharide with platelet-rich plasma exosomes assembled on chitosan/silk hydrogel sponge in a diabetic rat model, Int. J. Biol. Macromol. 117 (2018) 102–107.
[49] C. Wang, C. Liang, R. Wang, X. Yao, P. Guo, W. Yuan, Y. Liu, Y. Song, Z. Li, X. Xie, The fabrication of a highly efficient self-healing hydrogel from natural biopolymers loaded with exosomes for the synergistic promotion of severe wound healing, BIOMATER SCI-UK 8 (1) (2019) 313–324.
[50] X. Yao, W. Wei, X. Wang, L. Chenglin, M. Björklund, H. Ouyang, Stem cell derived exosomes: microRNA therapy for age-related musculoskeletal disorders, Biomaterials 224 (2019) 119492.
[51] C. Xia, Z. Zeng, B. Fang, M. Tao, C. Gu, L. Zheng, Y. Wang, Y. Shi, C. Fang, S. Mei, Q. Chen, J. Zhao, X. Lin, S. Fan, Y. Jin, P. Chen, Mesenchymal stem cell-derived exosomes ameliorate intervertebral disc degeneration via anti-oxidant and anti-inflammatory effects, Free Radic. Biol. Med. 143 (2019) 1–15.
[52] L. Luo, X. Jian, H. Sun, J. Qin, Y. Wang, J. Zhang, Z. Shen, D. Yang, C. Li, P. Zhao, M. Liu, Z. Tian, Y. Zhou, Cartilage endplate stem cells inhibit intervertebral disc degeneration by releasing exosomes to nucleus pulposus cells to activate Akt/autophagy, Stem cells 39 (4) (2021) 467–481.
[53] S. Cheng, X. Li, L. Lin, Z. Jia, Y. Zhao, D. Wang, D. Ruan, Y. Zhang, Identification of aberrantly expressed genes during aging in rat nucleus pulposus cells, STEM CELLS INT 2019 (2019) 2785207.
[54] D. Sakai, Y. Nakamura, T. Nakai, T. Mishima, S. Kato, S. Grad, M. Alini, M. V. Risbud, D. Chan, K.S. Cheah, K. Yamamura, K. Masuda, H. Okano, K. Ando, J. Mochida, Exhaustion of nucleus pulposus progenitor cells with ageing and degeneration of the intervertebral disc, Nat. Commun. 3 (2012) 1264.
[55] D. Sakai, G.B. Andersson, Stem cell therapy for intervertebral disc regeneration: obstacles and solutions, Nat. Rev. Rheumatol. 11 (4) (2015) 243–256.
[56] B. Zhu, L. Zhang, C. Liang, B. Liu, X. Pan, Y. Wang, Y. Zhang, Y. Zhang, W. Xie, B. Yan, F. Liu, H.K. Yip, X.Y. Yu, Y. Li, κStem cell-derived exosomes prevent aging-induced cardiac dysfunction through a novel exosome/lncRNA MALAT1/NF-B/TNF- signaling pathway, Oxid. Med. Cell. Longev. 2019 (2019) 9739258.
[57] M. Oh, J. Lee, Y.J. Kim, W.J. Rhee, J.H. Park, Exosomes derived from human induced pluripotent stem cells ameliorate the aging of skin fibroblasts, Int. J. Mol. Sci. 19 (6) (2018).
[58] P. Wang, Y. Yuan, W. Lin, H. Zhong, K. Xu, X. Qi, Roles of sphingosine-1-phosphate signaling in cancer, Cancer Cell Int. 19 (2019) 295.
[59] S. Panneer Selvam, R.M. De Palma, J.J. Oaks, N. Oleinik, Y.K. Peterson, R. V. Stahelin, E. Skordalakes, S. Ponnusamy, E. Garrett-Mayer, C.D. Smith, B. Ogretmen, Binding of the sphingolipid S1P to hTERT stabilizes telomerase at the nuclear periphery by allosterically mimicking protein phosphorylation, Sci. Signal. 8 (381) (2015) a58.
[60] Y. Shi, X.Y. Liu, Y.P. Jiang, J.B. Zhang, Q.Y. Zhang, N.N. Wang, H.L. Xin, Monotropein attenuates oxidative stress via Akt/mTOR-mediated autophagy in osteoblast cells, Biomedicine & pharmacotherapy = Biomedecine & pharmacotherapie 121 (2020) 109566.
[61] M. Trayssac, Y.A. Hannun, L.M. Obeid, Role of sphingolipids in senescence: implication in aging and age-related diseases, J. Clin. Invest. 128 (7) (2018) 2702–2712.
[62] Y. Li, Y. Guo, Y. Fan, H. Tian, K. Li, X. Mei, Melatonin enhances autophagy and reduces apoptosis to promote locomotor recovery in spinal cord injury via the PI3K/AKT/mTOR signaling pathway, Neurochem. Res. 44 (8) (2019) 2007–2019.
[63] X. Gao, J. Yang, Y. Li, M. Yu, S. Liu, Y. Han, X. Lu, C. Jin, S. Wu, Y. Cai, Lanthanum chloride induces autophagy in rat hippocampus through ROS-mediated JNK and AKT/mTOR signaling pathways, Metallomics : integrated biometal science 11 (2) (2019) 439–453.
[64] F.B. Feng, H.Y. Qiu, Effects of Artesunate on chondrocyte proliferation, apoptosis and autophagy through the PI3K/AKT/mTOR signaling pathway in rat models with

rheumatoid arthritis, Biomedicine & pharmacotherapy = Biomedecine & pharmacotherapie 102 (2018) 1209–1220.

[65] J. Zhang, J.X. Zhang, Q.L. Zhang, PI3K/AKT/mTOR-mediated autophagy in the development of autism spectrum disorder, Brain Res. Bull. 125 (2016) 152–158.

[66] X. Wang, Y.F. Fu, X. Liu, G. Feng, D. Xiong, G.F. Mu, F.P. Chen, ROS promote ox-LDL-induced platelet activation by up-regulating autophagy through the inhibition of the PI3K/AKT/mTOR pathway, Cell. Physiol. Biochem. : international journal of experimental cellular physiology, biochemistry, and pharmacology 50 (5) (2018) 1779–1793.